Book Section:
Han, YJ orcid.org/0000-0003-2141-3077, Li, LH orcid.org/0000-0003-4998-7259, Valavanis, A orcid.org/0000-0001-5565-0463 et al. (9 more authors) (2017) Development of Terahertz Frequency Quantum Cascade Lasers for the Applications as Local Oscillators. In: Pereira, MF and Shulika, O, (eds.) THz for CBRN and Explosives Detection and Diagnosis. NATO Science for Peace and Security Series B: Physics and Biophysics . Springer Netherlands , Dordrecht, Netherlands , pp. 123-134. ISBN 978-94-024-1093-8

https://doi.org/10.1007/978-94-024-1093-8_15

Development of terahertz frequency quantum cascade lasers for the applications as local oscillators

Y. J. Han[1,*], L. H. Li[1], A. Valavanis[1], N. Brewster[2], J. X. Zhu[1], R. Dong[1], P. Dean[1], L. Bushnell[2], M. Oldfield[2], A. G. Davies[1], B. Ellison[2], and E. H. Linfield[1]

[1]School of Electronic and Electrical Engineering, University of Leeds, Leeds LS2 9JT, UK

[2]Rutherford Appleton Laboratory, STFC, Harwell Oxford, Didcot OX11 0QX, UK

*y.han@leeds.ac.uk

Abstract We report the development of terahertz frequency quantum cascade lasers for applications as local oscillators. A range of active region designs and waveguide structures have been characterised in order to develop the devices for operation at high temperatures, with high output power and low dissipated power. Quantum cascade lasers based on a LO-phonon bound-to-continuum design emitting at 3.5 THz, suitable for the detection of hydroxyl, were fabricated with a double-metal (gold-gold) waveguide structure. These devices operated in continuous-wave up to 94 K, with an output power of 0.4 mW and dissipated power of 1.7 W at 10 K. A new, mechanically robust packaging and waveguide-integration scheme is also presented for operation outside laboratory environments, which further allows integration of quantum cascade lasers with terahertz waveguides, mixers and other system components. This integration scheme yielded a better beam quality, with a divergence of < 20°, compared to standard double-metal devices. Its impacts on the device performance, such as operating temperature range, spectral emission, output power and electrical properties, are presented.

Keywords: Terahertz, quantum cascade laser, local oscillator

1 Introduction

A range of chemical, biological, radiological and nuclear defence (CBRN) agents and explosives exhibit vibrational and rotational transitions at THz and mid-infrared (TERA-MIR) frequencies, and this has fuelled interest in developing materials, devices and systems for generating and detecting TERA-MIR radiation [1, 2]. Quantum-cascade lasers [3] (QCLs), in particular, are promising light sources in the terahertz (THz) spectral region [4]. After more than a decade's development, THz QCLs now cover the frequency range of 1 − 5 THz [5 − 7], and have been demonstrated as local oscillators in heterodyne receivers [8, 9]. Indeed, high resolution heterodyne spectroscopy is a powerful tool to measure molecular rotational lines and fine structure lines of atoms or ions. Many of these lines are located at the THz frequency region, including the hydroxyl (OH) rotational transitions at 1.8 THz, 2.5 THz, and 3.5 THz, and the atomic oxygen (OI) fine structure line at 4.7 THz, which are useful for exploring the Earth's atmosphere and interstellar media [10, 11]. Our aim is to use THz QCLs as local oscillators in airborne and satellite heterodyne spectrometers. For practical reasons, cooling of THz QCLs by liquid helium should ideally be replaced by a mechanical closed-cycle cooler. To be suitable as local oscillators in this configuration, THz QCLs have to simultaneously meet a number of essential requirements, such as maintaining a precise and targeted lasing frequency, high operating temperature, high optical output power, low dissipated power, good stability and a good beam profile. At the same time, a mechanically robust and reproducible scheme for integrating THz QCLs with external waveguides and mixers is required.

Here, we present the fabrication of THz frequency quantum cascade lasers (QCLs) emitting at 3.5 THz, as well as a new and robust integration scheme. The paper is organized as follows. In section 2, we discuss the details of the materials growth and device processing. In section 3, we present a comparison of THz QCLs with different active region designs and different waveguide structures, and the characterisation results of a high-performance 3.5 THz laser. In section 4, we introduce a new and robust integration scheme for THz QCLs [12], and present its effects on the beam profile, electrical and optical output properties. Finally, we discuss some further optimization of QCLs and integrations, and draw some conclusions.

2 Device fabrication and Characterisation

The QCLs used in this work are based on GaAs/AlGaAs materials. The QCL samples were grown on semi-insulating GaAs substrates using molecular beam epitaxy. For each wafer, a GaAs buffer layer and a 300 nm-thick $Al_{0.5}Ga_{0.5}As$ etch-stop layer were followed by a 700 nm-thick n+-GaAs contact layer doped

with Si to 2×10^{18} cm^{-3}. After those layers, the active region structure was grown repeatedly to a total thickness of 10 − 15 μm. On the top of the active region, a 50 nm-thick n+-GaAs contact layer was grown with a Si concentration of 5×10^{18} cm^{-3}.

QCL devices were processed according to the configuration of a semi-insulating-substrate-surface-plasmon (SISP) waveguide [4] or a double-metal (DM) waveguide [13]. For the SISP waveguide, laser ridges were defined by wet chemical etching. A 150 nm-thick AuGeNi electrical bottom contact layer was deposited beside the ridges and annealed at 400 °C for 1 minute. Two 10 μm-wide stripes of AuGeNi layers were deposited on the ridges as a top contact. The waveguide metal layers, Ti/Au (10/150 nm), were deposited on top of the laser ridges and annealed at 270 °C for 4 minutes. For the DM waveguide, Ti/Au of thickness 10/500 nm was deposited on top of the QCL wafer, and also on a second n+-GaAs acceptor wafer. The two wafers were then thermal compression bonded at the metallic interfaces. The substrate of the QCL wafer was lapped to 10 μm, and removed by selective wet chemical etching. Following wet-etching of the laser ridges, Ti/Au (10/150 nm) was deposited on the top. The substrate was thinned and metallised to improve thermal performance, and the ridges were then cleaved and Indium-soldered on the copper submounts.

For the light intensity–current–voltage (L–I–V) and spectral characterization, the devices were mounted on the cold finger of a helium-cooled cryostat and operated in continuous wave (CW) mode or in pulsed mode with 2-μs-long pulses at a repetition rate of 10 kHz. The laser emission was detected using a cooled Ge:Ga bolometer. The output power was calibrated using an absolute THz power meter (Thomas–Keating Instruments).

3 Experimental results of QCLs

In airborne or satellite heterodyne spectrometers, the dissipated power of THz QCLs should be below the cooling power of the closed-cycle cooler, which is typically several watts at 80 K and decreases at lower temperatures. A QCL with low dissipated power, high operating temperature and high output power is therefore desirable for the optimisation of spectrometer systems. Starting with a comparison of different active region designs and waveguide structures, we here identify a suitable design and present characterisation data for a high-performance device.

3.1 Comparison of active region designs

Comparison of different active region designs is not straight-forward since those designs normally have different lasing frequencies, doping concentration and

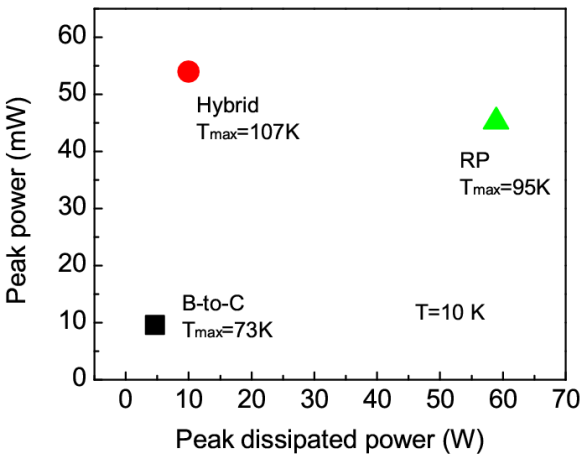

Fig. 1 Comparison of three active region designs. The devices have the same dimensions of 3000 μm × 150 μm, and were operated in pulsed mode

active region thickness. Material growth and fabrication processes also affect the device performance. In order to make the comparison easier, three commonly investigated designs lasing around 3.3±0.2 THz were grown and fabricated under similar conditions. The differences in doping concentration or total thickness can be implied by the device dissipated power and the output power.

In Fig. 1, the performance of QCL devices based on a bound-to-continuum (B-to-C), B-to-C with longitudinal-optical (LO) phonon extraction (hybrid) and resonant phonon (RP) designs are compared [14 − 16]. All three devices were processed into the SISP waveguide, cleaved to the same size of 3000 μm × 150 μm, and characterised in pulsed mode. The B-to-C design had the lowest dissipated power (4.6 W), which satisfies the requirement of the provided cooling power. However, it gave the lowest maximum operating temperature (73 K) and the lowest output power (9.7 mW), limiting its use as a local oscillator, especially at high temperatures. The RP design yielded a higher maximum operating temperature (95 K) and a higher output power (45.1 mW), but the dissipated power was much higher than the B-to-C design. In this case, the increased electrical power consumption generated much more Joule heating inside the RP structure, and limited the CW performance. The required cooling power for the RP design was about 60 W, which is out of the capability of typical closed-cycle coolers. Although the dissipated power can be lowered by decreasing the doping density or the device size, it is at the expenses of the output power. The hybrid design was found to provide the benefits of both the B-to-C design and the RP design; it yielded the highest output power (54 mW) and the highest maximum operating temperature (107 K) of the three structures, and at the same, the dissipated power was comparable to the B-to-C design. Therefore, the hybrid design is identified as a promising choice to meet local oscillator requirements.

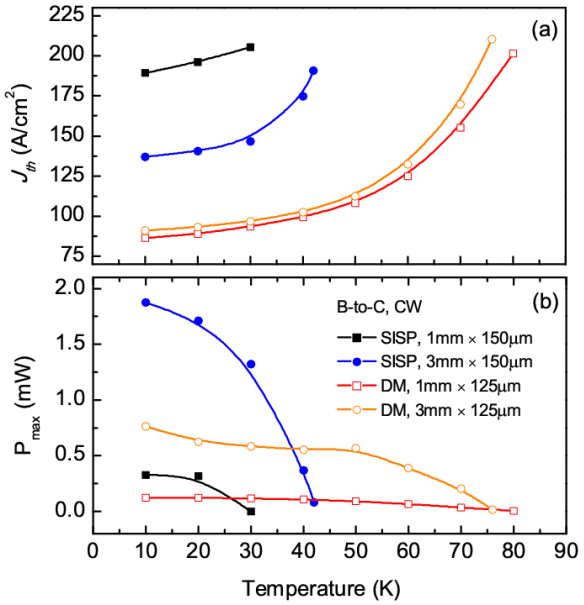

Fig. 2 Temperature evolution of (a) threshold current density, J_{th}, and (b) the maximum output power, P_{max}, of THz QCLs with different waveguide configuration. The devices were operated in CW mode

3.2 Comparison of waveguide structures

Two waveguide configurations, SISP and DM, are normally used for THz QCLs [4, 13]. In the SISP waveguide, a semi-insulating substrate and a thin confinement layer lowers the waveguide loss at the expense of the confinement factor (and hence net gain) of guided modes. In the DM waveguide, the optical field is almost entirely confined inside the active region by two metal layers, but this strict confinement results in widely divergent emission.

Fig. 2 shows the temperature dependence of the CW threshold current density, J_{th}, and maximum output power of two pairs of laser ridges process with a SISP waveguide and a DM waveguide, respectively. The only difference between the devices in each pair is the length, being 1 mm for one device and 3 mm for the other. The width of devices in each pair is the same, 150 μm for the SISP devices and 125 μm for the DM devices. As can be seen, the effects of employing double-metal waveguide are significant. Increases of more than 30 K in the maximum operating temperature were observed, with the output power only degrading significantly for temperatures higher than 50 K. Although the output power of the DM devices was only at half the level obtained with the SISP devices at 10 K, the slow thermal damping rate of DM devices resulted in higher optical power at elevated temperatures. With the increase of device length, the mirror loss is lowered. As a result, a reduction in threshold current density was observed for both waveguide structures, and the decrease of the threshold current is more obvious for the SISP

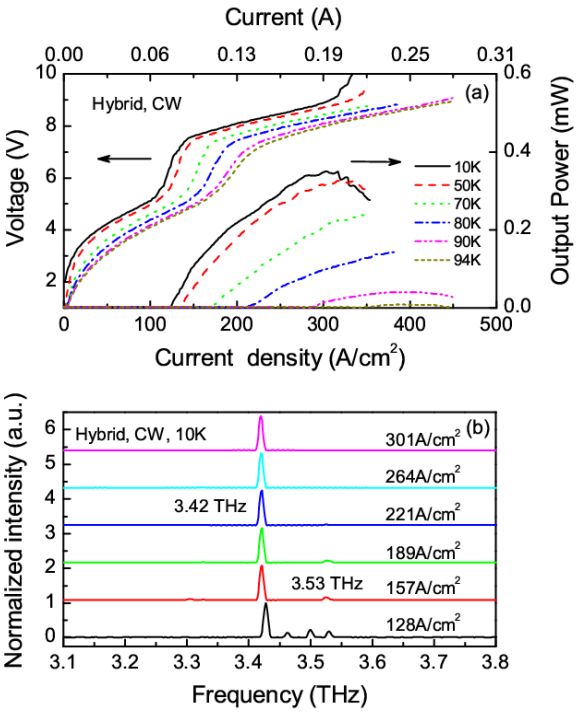

Fig. 3 L–I–V curves at different temperatures and emission spectra at 10 K. The device was operated in CW mode

device due to the smaller optical mode confinement factor. The longer devices emitted higher optical output power, but also dissipated more electrical power. This caused increased Joule heating, limiting the maximum operating temperature of the long DM QCL to 4 K lower than that of the short device. Overall, the DM QCLs showed better temperature performance than the SISP QCLs, i.e., higher output power at high temperatures, and therefore, the DM waveguide is preferred to be employed to develop QCLs for local oscillator applications.

3.3 QCLs lasing at 3.5 THz

The hybrid active region plus the DM waveguide have been identified as the optimum choice for THz QCLs for use as local oscillators, owing to the good temperature performance and low dissipated power. Based on the hybrid design shown in Fig. 1, the active region was modified to shift the gain spectra from 3.1 THz to 3.5 THz. During the material growth, the total thickness was also increased to 15 μm and the doping concentration in the active region was optimized. The device was processed into DM waveguide structure with dimensions of 500 μm × 125 μm, and driven in CW mode.

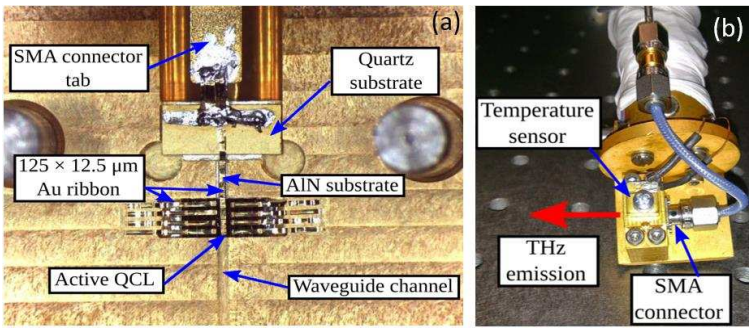

Fig. 4 (a) Interior of bottom half of waveguide block, and (b) exterior of QCL waveguide block (Reproduced from Valavanis et al. 2015)

Fig. 3 shows L–I–V characteristics obtained at different temperatures, as well as the emission spectra at 10 K. This optimised design yielded a considerable improvement in the operating temperature and the output power. Compared with the B-to-C design (Fig. 2), the maximum operating temperature increased from 80 K to 94 K, and the output power from 0.13 mW to 0.35 mW. The dissipated power was 1.7 W, higher than the B-to-C design, but within the requirement of cooling power. Furthermore, this device provided more than 0.1 mW output power with a dissipated power of 2.0 W at 80 K. Note that the output power presented here is an underestimate of the generated THz power, since the collection efficiency is not considered. The emission spectra was observed from 3.42 to 3.53 THz, and covered the target frequency of 3.5 THz.

4 Integration of QCLs with waveguide blocks

QCLs in double-metal waveguides yield good thermal performance, as demonstrated above, but also poor far-field beam quality and wide beam divergence. Although the far-field beam can be improved by using techniques such as device patterning approaches [17, 18] or assemblies of antennas or lenses [19, 20], their reproducibility and mechanical robustness have not been demonstrated. Here, we present a waveguide block integration scheme for THz QCLs [12], and investigate its effects on the beam profile and laser performance.

4.1 Waveguide integration scheme

In the waveguide-integration scheme [12], a double-metal QCL was mounted within a copper heat-sink enclosure containing a rectangular cross-section metallic

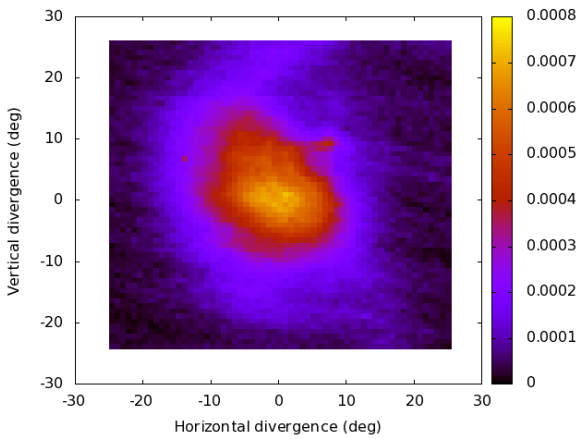

Fig. 5 Two dimensional image of far-field beam profile (Reproduced from Valavanis et al. 2015)

waveguide. The QCL was based on the B-to-C design, as described in Fig. 2, and the device length was adjusted to 980 μm. The QCL chip contained 13 independent ridges although only one of them was connected electrically.

Fig. 4 shows the waveguide block with a QCL integrated inside. The waveguide block was precision-machined directly into a Cu block by mechanical microfabrication techniques, with a channel of cross-sectional dimensions 300 μm × 150 μm, including a cavity for the positioning of a QCL. The QCL chip was mounted in the cavity by using an indium foil to ensure a good thermal contact. The output facet of the central QCL ridge was aligned with the waveguide aperture. A Au ribbon bond was used to provide an electrical connection to the top contact of the QCL through a small Au-plated strip of AlN and a Au-plated quartz substrate secured to the Cu block by high conductivity silver-loaded epoxy. The complete assembled block was mounted into a cryostat, and the electrical bias was supplied through a subminiature-A (SMA) connector on the rear of the block. The temperature was monitored at the top of the block.

To measure the far-field beam profile of the integrated QCL, a Golay detector with an entrance aperture of 1 mm diameter was scanned linearly in two dimensions at a distance 32.4 mm from the laser facet. The laser was driven using a continuous 30 Hz square wave, and operated at a heat-sink temperature of 30 K. As shown in Fig. 5, an approximately Gaussian single-lobed profile was observed. The full-width at half-maximum (FWHM) in the growth and in-plane directions is 20° and 17°, respectively [12]. This is comparable to the divergence obtained previously by patterning the QCL or through the use of device-integrated antenna structures or lenses, and the ‘ringing’ that is commonly associated with the beam profiles of normally mounted DM QCLs is removed entirely.

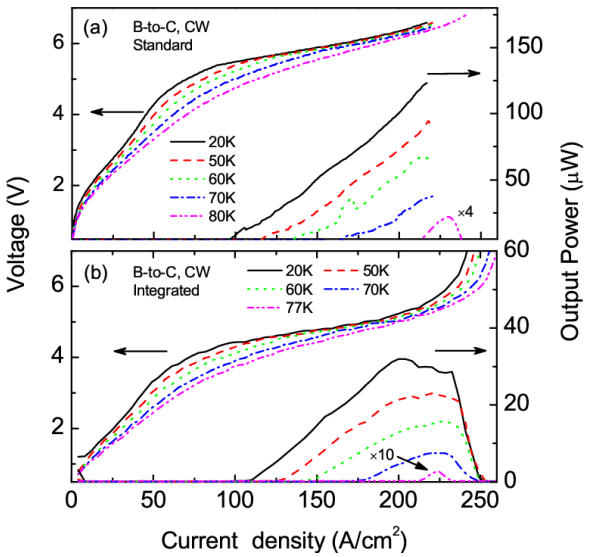

Fig. 6 L–I–V curves of (a) standard mounted and (b) integrated QCLs at different temperatures. The lasers operated in CW mode

4.2 Comparison with standard mounted QCLs

The temperature performance and the spectra of the integrated QCL have been compared with those of a standard mounted QCL, in order to investigate the effects of the waveguide block upon the maximum operating temperature, output power, dissipated power and electrical connections. The standard mounted QCL used for this comparison is the short DM device reported in Fig. 2, with a length of 1mm being the only difference to the QCL integrated in the waveguide block (length 980 μm).

Fig. 6 shows the L–I–V curves of the standard QCL and the integrated QCL at different temperatures. In comparison, the I–V curves of the two devices are similar, expect for a drop in the applied voltage of the integrated QCL. At a temperature of 20 K, the voltage drop, ΔV, can be fitted to the function $\Delta V = I \times R_s + V_s$, from which a series resistance $R_s = 1.2\ \Omega$ and an addition voltage drop $V_s = 0.9$ V are obtained. This implies that the integration scheme improved the electrical connections and will lead to a reduction in dissipated power. The integrated QCL yielded a threshold current density of 102 A/cm^2 at 20K and maximum operation temperature of 77 K, slightly worse compared with 89 A/cm^2 and 80 K of the standard device. This can be attributed to a small increase in the thermal resistance of the waveguide block and cryostat. The integrated device was also found to have a reduction in the output power to 32 μW, about 25% of the standard device. Since there was no significant change in I–V curves, the drop in the output power, has been ascribed to a mismatch between the transverse mode profile of the laser

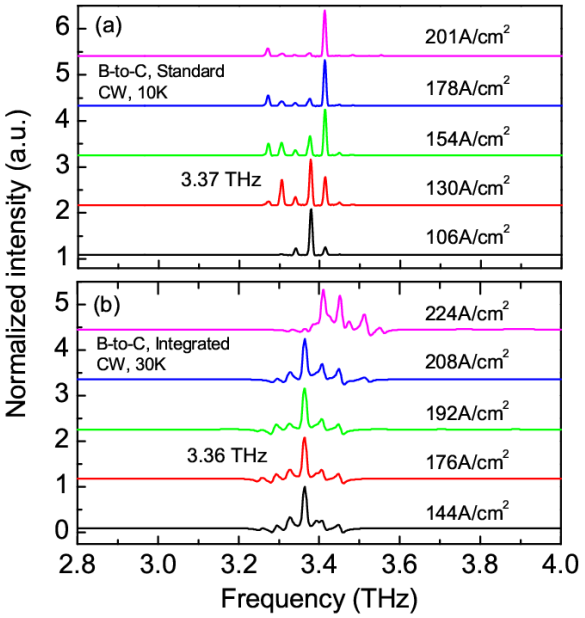

Fig. 7 Emission spectra of (a) standard mounted and (b) integrated QCLs. The lasers were operated in CW mode

cavity and that of the relatively wide rectangular waveguide, and also between the waveguide aperture and free space [12].

Fig. 7 shows the emission spectra of the standard and integrated QCLs. Multi-mode emission was observed in both cases, with the same central frequency of 3.4 THz and similar spectral bandwidth of ~120 GHz. The side modes emitted from the integrated device were broadened and attenuated, which could be related with the waveguide channel in the block, rather than the QCL itself.

Overall it can be seen that this integration scheme can improve the emission beam quality significantly, as well as the electrical connection, while not introducing significant perturbation to the internal properties of the laser itself. The issues related to the reduction of the output power arising from the mismatch between the transverse mode profile of the laser cavity and that of the waveguide, will be addressed in the next design.

Conclusion

We have reported the development and optimisation of terahertz frequency quantum cascade lasers for applications as local oscillators. A device consisting of a 'hybrid' active region design based on a bound-to-continuum transition with longitudinal-optical (LO) phonon extraction, plus a double metal waveguide structure, has been identified as a promising choice. A high-performance QCL based on this design and emitting at 3.5 THz was fabricated, and shown to operate in

CW mode up to a temperature of 94 K, with a low temperature output power of ~0.4 mW and dissipated power of 1.7 W. Single frequency emission and better thermal management will be considered in the next device iteration. In addition, a new waveguide integration scheme for THz QCLs was demonstrated based on a highly reproducible precision-micromachining technique. This approach improved the electrical connections and yielded a considerably improved beam divergence of <20°, whilst maintaining a low threshold current and good operating temperature range. A higher output power can be expected by integrating an optimized QCL with a new design of waveguide block.

Acknowledgments We acknowledge financial support from the EPSRC (UK) 'COTS' programme, the ERC grant 'NOTES' and 'TOSCA', NERC (UK), the European Space Agency, and the CEOI-ST. AGD and EHL also acknowledge support from the Royal Society and the Wolfson Foundation. PD acknowledges support from EPSRC (UK).

References

1. http://www.tera-mir.org,
2. P. Dean, A. Valavanis, J. Keeley, K. Bertling, Y. L. Lim, R. Alhathlool, A. D. Burnett, L. H. Li, S. P. Khanna, D. Indjin, T. Taimre, A. D. Rakić, E. H. Linfield, A. G. Davies, Terahertz imaging using quantum cascade lasers - review of systems and applications, J. Phys. D 47, 374008 (2014),
3. J. Faist, F. Capasso, D. L. Sivco, C. Sirtor, A. L. Hutchinson, A. Y. Cho, Quantum Cascade Laser, Science 264, 553–556 (1994),
4. R. Köhler, A. Tredicucci, F. Beltram, H. E. Beere, E. H. Linfield, A. G. Davies, D. A. Ritchie, R. C. Iotti, F. Rossi, Terahertz semiconductor-heterostructure laser, Nature 417, 156–159 (2002),
5. L. Li, L. Chen, J. Zhu, J. Freeman, P. Dean, A. Valavanis, A. G. Davies E.H. Linfield, Terahertz quantum cascade lasers with >1 W output powers, Electron Lett. 50, 309-311 (2014),
6. C. Walther, M. Fischer, G. Scalari, R. Terazzi, N. Hoyler, J. Faist, Quantum cascade lasers operating from 1.2 to 1.6 THz, Appl. Phys. Lett. 91, 131122 (2007),
7. C. W. Chan, Q. Hu, J. L. Reno, Ground state terahertz quantum cascade lasers, Appl. Phys. Lett. 101, 151108 (2012),
8. J. R. Gao, J. N. Hovenier, Z. Q. Yang, J. J. A. Baselmans, A. Baryshev, M. Hajenius, T. M. Klapwijk, A. J. L. Adam, T. O. Klaassen, B. S. Williams, S. Kumar, Q. Hu, J. L. Reno, Terahertz heterodyne receiver based on a quantum cascade laser and a superconducting bolometer, Appl. Phys. Lett. 86, 244104 (2005),

9. H. W. Hubers, S. G. Pavlov, A. D. Semenov, R. Köhler, L. Mahler, A. Tredicucci, H. E. Beere D. A. Ritchie, E. H. Linfield, Terahertz quantum cascade laser as local oscillator in a heterodyne receiver, Opt Express 13, 5890-5896 (2005),
10. R. G. Prinn, J. Huang, R. F. Weiss, D. M. Cunnold, P.J. Fraser, P.G. Simmonds, A. McCulloch, C. Harth, P. Salameh, S. O'Doherty, R.H.J. Wang, L. Porter, B. R. Miller, Evidence for substantial variations of atmospheric hydroxyl radicals in the past two decades, Science 292, 1882-1888, (2001),
11. R. T. Boreiko1, A. L. Betz1, Heterodyne Spectroscopy of the 63 μm O I Line in M42, The Astrophysical J. Lett. 464, L83 (1996),
12. A. Valavanis, Y. J. Han, N. Brewster, P. Dean, R. Dong, L. Bushnell, M. Oldfield, J. X. Zhu, L. H. Li, A. G. Davies, B. Ellison, E. H. Linfield, Mechanically robust waveguide-integration and beam shaping of terahertz quantum cascade lasers, Electron. Lett. 51, 919-920 (2015),
13. B. S. Williams, S. Kumar, H. Callebaut, Qing Hu, J. L. Reno, Terahertz quantum-cascade laser at lambda approximate to 100 mu m using metal waveguide for mode confinement, Appl. Phys. Lett. 83, 2124-2126 (2003),
14. G. Scalari, L. Ajili, J. Faist, H. Beere, E. H. Linfield, David Ritchie, A. G. Davies, Far-infrared (lambda similar or equal to 87 μm) bound-to-continuum quantum-cascade lasers operating up to 90 K, Appl. Phys. Lett. 82, 3165-3167 (2003),
15. M. Wienold, L. Schrottke, M. Giehler, R. Hey, W. Anders, H. T. Grahn, Low-voltage terahertz quantum-cascade lasers based on LO-phonon-assisted interminiband transitions, Electron. Lett. 45, 1030-1040 (2009),
16. S. Fathololoumi, E. Dupont, C. W. Chan, Z. R. Wasilewski, S. R. Laframboise, D. Ban, A. Mátyás, C. Jirauschek, Q. Hu, and H. C. Liu, Terahertz quantum cascade lasers operating up to ~ 200 K with optimized oscillator strength and improved injection tunneling, Opt. Express 20, 3866-3876 (2012),
17. M. I. Amanti, M. Fischer, G. Scalari, M. Beck, J. Faist, Low-divergence single-mode terahertz quantum cascade laser, Nature Photonics 3, 586-590 (2009),
18. N. F. Yu, J. Fan, and Q. J. Wang, C. Pflügl, L. Diehl, T. Edamura, M. Yamanishi, H. Kan, F. Capasso, Small-divergence semiconductor lasers by plasmonic collimation, Nature Photonics 2, 564-570 (2008),
19. M. I. Amanti, M. Fischer, C. Walther, G. Scalari, M. Beck, J. Faist, Horn antennas for terahertz quantum cascade lasers, Electron Lett 43, 573-574 (2007),
20. A. W. M. Lee, Q. Qin, S. Kumar, B. S. Williams, Q. Hu, J. L. Reno, High-power and high-temperature THz quantum-cascade lasers based on lens-coupled metal-metal waveguides, Opt. Lett. 32, 2840-2842 (2007).